Facies Analyses and Depositional Environments of the Carbonates and Ironstones-Bearing Succession of Um Himar Formation, Turabah Area, Saudi Arabia

Ali A. Mesaed
Geo-Exploration Techniques Department, Faculty of Earth Sciences, King Abdulaziz University, Jeddah, Saudi Arabia | Geology Department, Faculty of Sciences, Cairo University, Giza, Egypt
alimesaed@yahoo.com (corresponding author)

Rushdi J. Taj
Petroleum Geology and Sedimentology Department, Faculty of Earth Sciences, King Abdulaziz University, Jeddah, Saudi Arabia
rtaj@kau.edu.sa

Mohamed Gameil
Petroleum Geology and Sedimentology Department, Faculty of Earth Sciences, King Abdulaziz University, Jeddah, Saudi Arabia | Geology Department, Faculty of Sciences, Cairo University, Giza, Egypt
mgsayed@kau.edu.sa

Ahmad S. Tayeb
Petroleum Geology and Sedimentology Department, Faculty of Earth Sciences, King Abdulaziz University, Jeddah, Saudi Arabia
astayeb@kau.edu.sa

Mohamed I. Matsah
Structural Geology and Remote Sensing Department, Faculty of Earth Sciences, King Abdulaziz University, Jeddah, Saudi Arabia
momatsah@kau.edu.sa

Received: 10 March 2026 | Revised: 18 April 2026 and 8 May 2026 | Accepted: 9 May 2026

 DOI: https://doi.org/10.48084/etasr.18651

ABSTRACT

The present study investigates facies analysis and depositional environments of the carbonate- and ironstone-bearing succession of the Um Himar Formation in the Turabah area. The study area is located in the southwestern part of the Arabian Shield of Saudi Arabia. Geologically, the area includes Arabian shield rocks that are overlain by the studied tertiary sedimentary succession of the Um Himar Formation. Tertiary basaltic flows are present and terminate the Tertiary succession. The Um Himar Formation is composed of four main units: Unit 1: Metavolcanics-Silicified Carbonate; Unit 2: Glauconitic Yellow Clays-Dolostone; Unit 3: Green Clays-Iron Ore; and Unit 4: Tertiary basic volcanic flows (Harrat). Field and microscopic investigations of these units revealed nine facies and related subfacies. Unit 1 is composed of andesitic tuffs and silicified dolostone and represents part of the greenstone belt of the Bidah Group to the west of the study area. It is composed of successive cycles of green glauconitic clays that grade into yellow dolomitic mudstones and dolostones. The cyclic pattern indicates the beginning of deposition in slightly deeper (dysaerobic) conditions. During the progressive shoaling of the depositional environments and a decrease in the volcaniclastic input, the silicified carbonates were deposited, which indicates restriction of the depositional environment and an increase in the alkalinity and formation of evaporitic

cherty bands. Unit 2 represents a new transgressive cycle that begins with green celadonitic clays that were formed during the synsedimentary authigenesis instead of the deposited basic tuffs during transgressive time. During the progressive shoaling, thinly bedded dolostones were deposited in restricted environments. Unit 3 represents reddish brown to black massive ironstones, just terminated by oxidized green celadonitic clays. These ironstones were formed by diagenetic devitrification and hematitization of the underlying green clays and formation of reddish brown silicified hematitic iron ore horizon. Basaltic volcanic flows led to the formation of the topmost Unit 4 of the succession.

Keywords-Um Himar Formation; carbonates, ironstones; volcaniclastics

I. INTRODUCTION

A. Geologic Setting

The Gabal Um Himar is located 6 km northeast of Turabah Government, AT Taif city, west-central Saudi Arabia, as shown in Figures 1 and 2. It consists of intrusive granites, granodiorite, and quartz diorite overlain by weathered rocks (saprolite horizon) and the Tertiary basaltic flows (Harrat). In areas near the Gabal Um Himar, the intrusive rocks are overlain by bedded greenish black metavolcanics and related volcaniclastics, which are directly overlain by the sedimentary succession of the Um Himar Formation. The section of the Um Himar Formation is capped by black Tertiary basaltic flows of Harrat Hadan, which covers a vast area to the north and northeast of the Turabah area.

Authors in [1] described the geologic map of the study area, Gabal Um Himar, and the collection of turtle remains (Order Chelonia) from the latter. They also conducted the mapping and description of the Um Himar Formation as a part of the 1:100,000-scale map. Authors in [3] discussed the stratigraphic section of the Gabal Um Himar area and reported the presence of fish fossils and oolitic iron ore beds in the lower part of the section. It was found that the Um Himar Formation consists of three members: a basal ferruginous mudstone, a middle fossiliferous interbedded mudstone and shale, and an upper dolomitic limestone. Moreover, the Paleocene Pycnodont fishes from the Gabal Um Himar and Harrat Hadan areas around Turabah city were studied, and a geologic map was designed. Based on this map, the rock units of the Gabal Um Himar were subdivided into the metavolcanics, granites, the Tertiary sedimentary succession of Um Himar Formation, and finally the basaltic lava flows (harrat). The map described a vast area occupied by black bedded metamorphosed Precambrian metavolcanics as Tertiary basic volcanics (Harrat), which are completely different from each other in lithology, field relations, and age.

Field observations enable readjustment of the rock units according to the designed geologic map, as shown in Figure 2(a), into the following: 1) Granite, which is the oldest rock unit in the study area, 2) the metavolcanics, which present faulted down against the studied sedimentary sequence of Um Himar Formation (Figure 3) directly without any erosional contact with the underlying formation.

B. Aims and Objectives

The main goal of this study is to characterize the carbonate-ironstones-bearing succession of the Um Himar Formation at the Gabal Um Himar. The objectives of the study are:

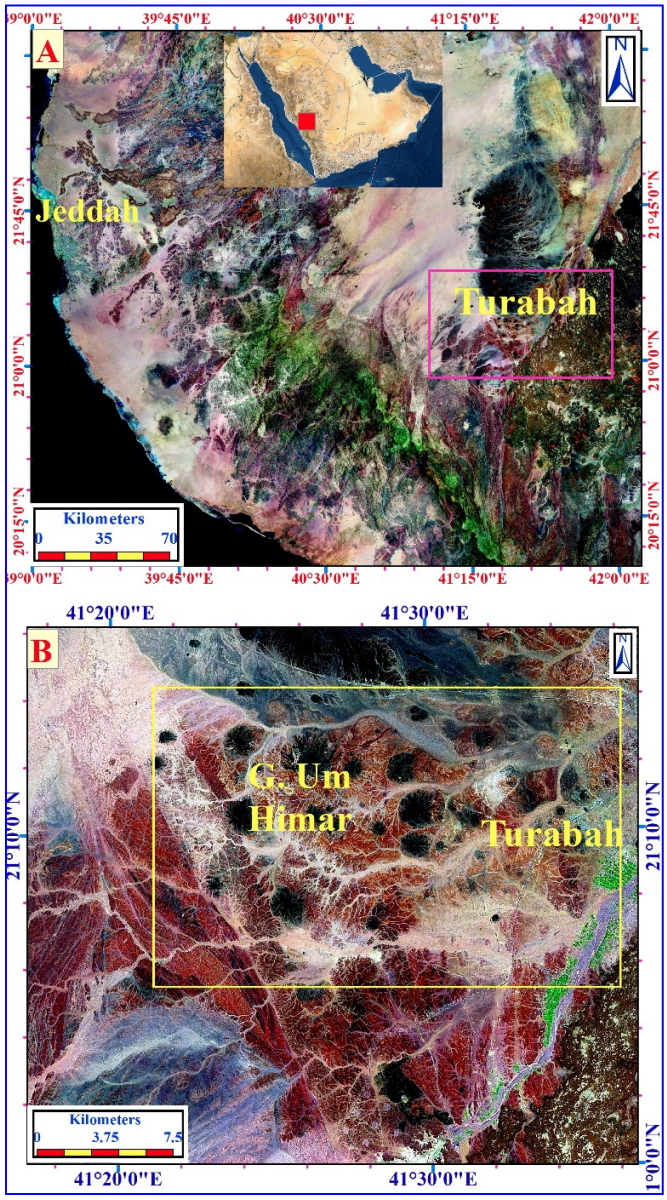

Fig. 1. (a) Regional satellite image of Makkah District showing the location of the Turabah area; (b) detailed satellite image of the Turabah area.

- Stratigraphic setting: Establish the stratigraphic framework and confirm its equivalence to the Oligo-Miocene Ash Shumaysi and Usfan formations [3].
- Facies analysis: Conduct a detailed lithofacies analysis to identify depositional patterns and variations.

- Paleoenvironmental reconstruction: Interpret the depositional environment and paleogeographic evolution of the succession.

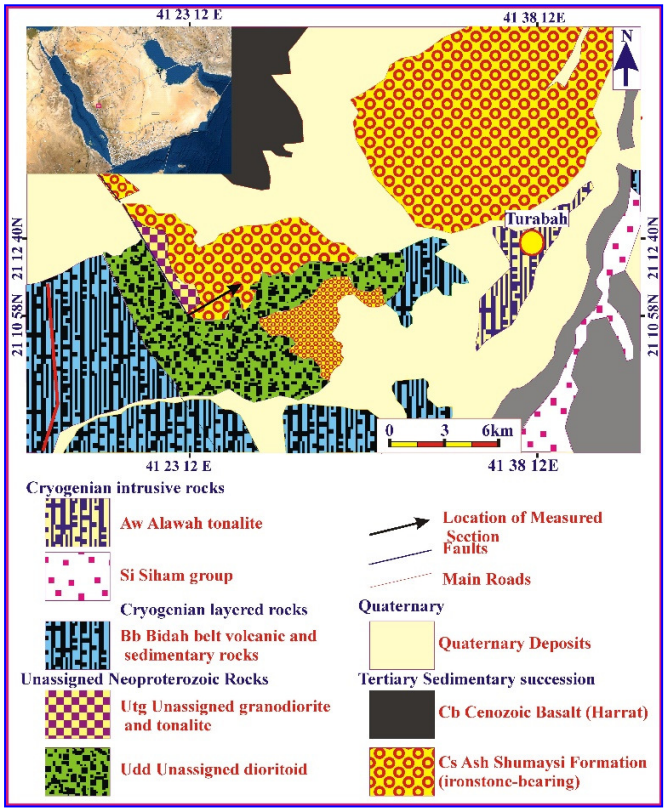

Fig. 2. Geologic map of the Turabah area based on [2].

The Paleocene-Tertiary just overlies a Precambrian Arabian Shield rock; however, the present study did not observe any hiatus or unconformity surface between this succession and the underlying metavolcanics. The succession of the Um Himar Formation was assigned as the granitic rocks, which are highly weathered. A thick saprolite horizon is observed along the contact between these rocks and the overlying Tertiary basaltic flows. The Khormah Formation between the Um Himar Formation and the Precambrian basement rocks in an area about 3 km southeast of the Gabal Um Himar was described in [1].

II. MATERIALS AND METHODS

A total of 30 representative hand samples were collected from different stratigraphic units of the study area. The samples were selected based on lithological variability and field relationships. The locations of the collected samples are displayed in the stratigraphic section of Figure 3 (U1, U2,…). Thirty standard thin sections were prepared from all samples following conventional petrographic procedures. Detailed petrographic analysis was conducted using transmitted light microscopy to identify mineralogical composition, textures, and diagenetic processes. High-resolution photomicrographs of the thin sections were captured, systematically documented, and compiled into photographic plates. In addition, organized photomontages were produced to illustrate key petrographic features and support microfacies interpretation. Finally, integrated field observations with microscopic data were conducted to improve the interpretation of depositional environments and sediment–volcanic interactions.

III. RESULTS

The detailed field observations and measurements of the stratigraphic succession of the Gabal Um Himar area help subdivide the exposed rock units of the area into four different units and related facies and subfacies, as presented in Table I.

A. Precambrian Metavolcanics-Silicified Carbonate (Unit 1)

This unit is well exposed in the extreme western part of the study area. It is faulted down against the underlying granite and includes two main facies: F1 and F2.

1) Bedded Choritized Metavolcanic Facies (F1)

These facies are composed of black metavolcanics that comprise sheared basalts, andesite, and schist, as depicted in Figures 4(a) and (b).

TABLE I. DIFFERENT UNITS AND RELATED FACIES AND SUBFACIES OF THE GABAL UM HIMAR

Unit	Facies and subfacies	General characteristics	Depositional setting
Unit 1	Bedded choritized metavolcanic facies (F1), yellow silicified carbonates facies (F2)	Interbedded chloritic andesitic tuffs and andesitic flows. Interbedded dolostones and chert bands	Volcanic arc (Arabian Shield rocks, restricted lagoons
Unit 2	Yellowish green glauconitic mudstone-carbonate facies (F3), chertified dolostone facies (F4), red ferruginous carbonate facies (F5)	Green clays, dolostone, and chertified dolostone interbeds	Shallow marine setting of general shallowing upward and restriction of depositional environments.
Unit 3	Slightly oxidized green clays (F7a), highly oxidized green clays-ironstone (F7b), highly devitrified celadonitic clays (F8), Ironstone facies (F9), yellowish green subfacies (F9a), reddish yellow subfacies (F9b), highly silicified-chertified (devitrified) subfacies (F9c), reddish brown ironstone subfacies (F9d)	Green and yellowish green celadonitic calys show progressive and subsequent stages of hematitization and formation of ironstone horizons	Initial transgression and formation of green clays with progressive shoaling; syn; post depositional diagenetic oxidation; and formation of ironstone beds with thin devitrified tuffs (chert bands)
Unit 4	Successive interbedded tuffaceous mudstones, siltstones, and basalt (Figures 3, 12(e)). Towards the upper parts, it is composed of basalts of variable crystal sizes and colors	Interbedded volcanic ash and basaltic flows	Marginal rift-related volcanic activities

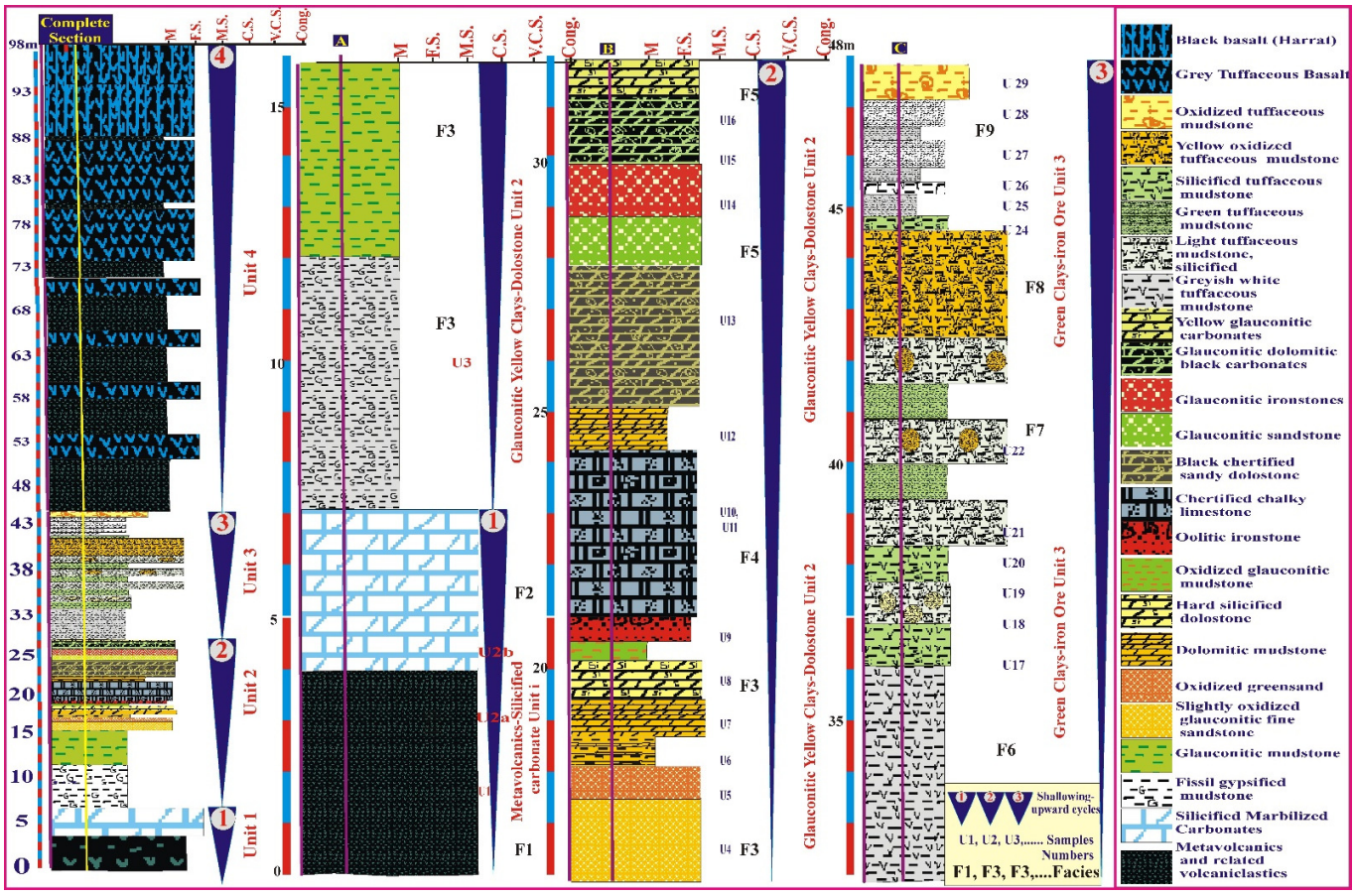

Fig. 3. Detailed stratigraphic section of Um Himar Formation in the Gabal Um Himar.

The microscopic description of this metavolcanics revealed its composition from highly chloritized andesitic rock, which comprises intensely chloritized amphiboles and plagioclases with some minor black iron oxide patches as well as calcite crystals, as portrayed in Figures 4 (c) and (d). These facies represent the uppermost part of the Arabian shield rocks and part of the Wadi Bidah volcano-sedimentary unit [2], and they are of oceanic affinity.

2) Yellow Silicified Carbonates Facies (F2)

The black metavolcanics of facies (F1) are directly overlain by bedded yellow silicified carbonate, as shown in Figures 3 and 4(e). Microscopically, these carbonates are composed mainly of coarse crystalline blocky calcite stained with some red iron oxides. The coarse crystalline calcite crystals show evidence supporting their formation by the diagenetic crystallization of the microcrystalline calcite crystals, as displayed in Figure 4(f). These facies represent carbonate-hosted volcaniclastics and are formed during periods of cessation of volcaniclastic input.

B. Glauconitic Yellow Clays-Dolostone (Unit 2)

1) Yellowish Green Glauconitic Mudstone-Carbonate Facies (F3)

These facies are present just overlying the silicified carbonate horizon (Figure 3). They are composed of successive small cycles of yellowish green glauconitic mudstone-siltstone and yellow carbonate beds. The yellowish green glauconitic mudstone-carbonate facies (F3) is composed of successive cycles, with each cycle beginning with yellow glauconitic mudstones that grade upward into egg-yellow limonitic mudstones and terminating with egg-yellow dolostones. These cycles represent deposition under water level fluctuation. Each of these cycles starts with the deposition of mudstone during a period of high clastic input. The deposited mud was progressively glauconitized along the sediment-water interface [4]. During the diagenetic processes, the glauconitic grains become progressively oxidized, giving rise to amorphous iron-oxyhydroxides [5]. The ultimate stage of shoaling is dominated during periods of low clastic input and deposition of Fe, Mg-rich lime mud, and formation of dolostone beds in the topmost parts of the cycles. The microscopic description of these facies led to the recognition of the following petrographic lithotypes:

a) Glauconitic Siltstone/Ironstone Lithotype

This lithotype is composed of grey and green glauconitic mudstone, as shown in Figure 4(g). This glauconitic mudstone contains thin hematitic glauconitic siltstone interbeds, as DEPICTED in Figure 4(h). Microscopically, it is composed of silt-sized quartz grains and small hematitized glauconitic grains within hematitic/goethitic cement. The quartz grains are highly corroded and embayed by the enclosing hematitic cement. The hematite cement was formed by the diagenetic recrystallization

of the associated amorphous blood-red iron-oxhydroxide, as presented in Figure 4(h). There is strong evidence supporting the processes of progressive corrosion and embayment of the quartz grains by the enclosing hematite cement. This occurs due to the formation of large patches and domains of goethite and hematite instead of the corroded and embayed quartz grains, and subsequently the formation of wide areas of hematite and goethite, which contain very small, irregular, highly embayed, and corroded quartz grains.

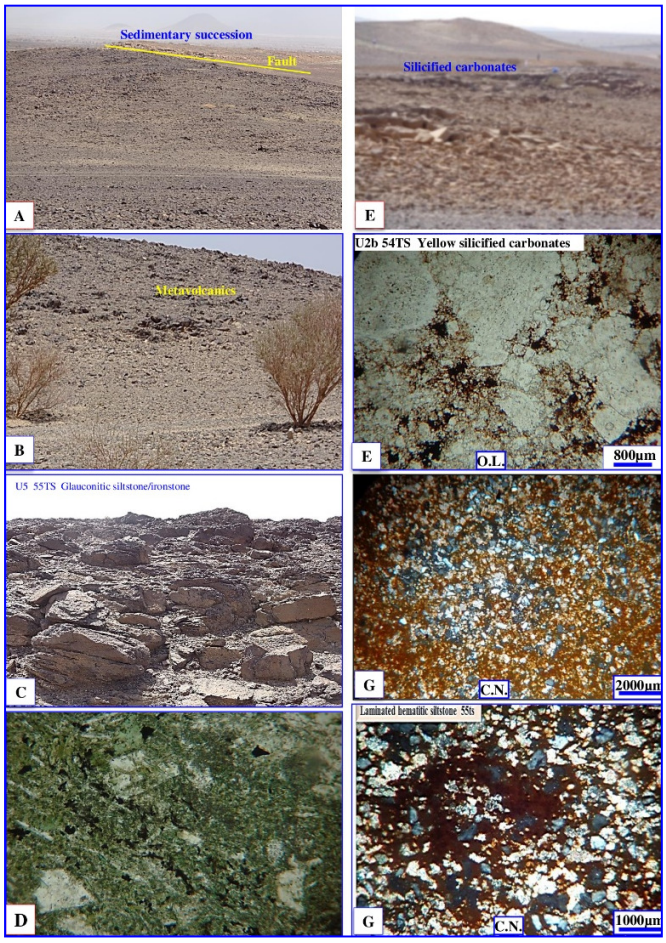

Fig. 4. (a and b): Different rock units of the stratigraphic section I; (c): bedded metavolcanics of Unit 1; (d): green chloritized metavolcanics of the lower part of section I; (e): bedded silicified carbonates of Unit 1; (f): crystalline iron-rich carbonates of the lower part of section I; (g): hematitic glauconitic siltstone of the lower part of section I; (h): black hematite cement formed by the diagenetic recrystallization of the associated amorphous blood-red iron-oxyhydroxides. O.L:. Ordinary Light, C.N.: Crossed Nicols.

b) Hematitic Lime Mud/Wackestone Lithotype

The glauconitic hematitic siltstone lithotype is overlain by a new cycle that begins with yellow dolomitic mud and is terminated with hematitic lime mud/wackstone, as shown in Figure 5(a). Microscopically, this lithotype is composed of microcrystalline calcite (micrite) stained with iron-oxyhydroxides and hematite. Some patches are composed of coarse calcite aggregates.

c) Egg-Yellow Oxidized Glauconitic Clays

This ironstone is present in a new cycle composed of basal green glauconitic mudstone, which is overlain directly by yellowish brown glauconitic siltstone (ironstone, Figure 5(b)). It is mainly composed of highly hematitized glauconitic clays, which oxidized into blood-red iron oxyhydroxides and hematite with small relicts of highly embayed quartz grains, as depicted in Figure 5(c). The glauconitic clays demonstrate progressive and subsequent stages of oxidation, dehydration, and recrystallization, as well as formation of blood-red and brown iron oxyhydroxide, goethite, and hematite, as illustrated in Figure 5(d). Black hematite patches were observed within the amorphous iron oxyhydroxides (Figure 5(e)).

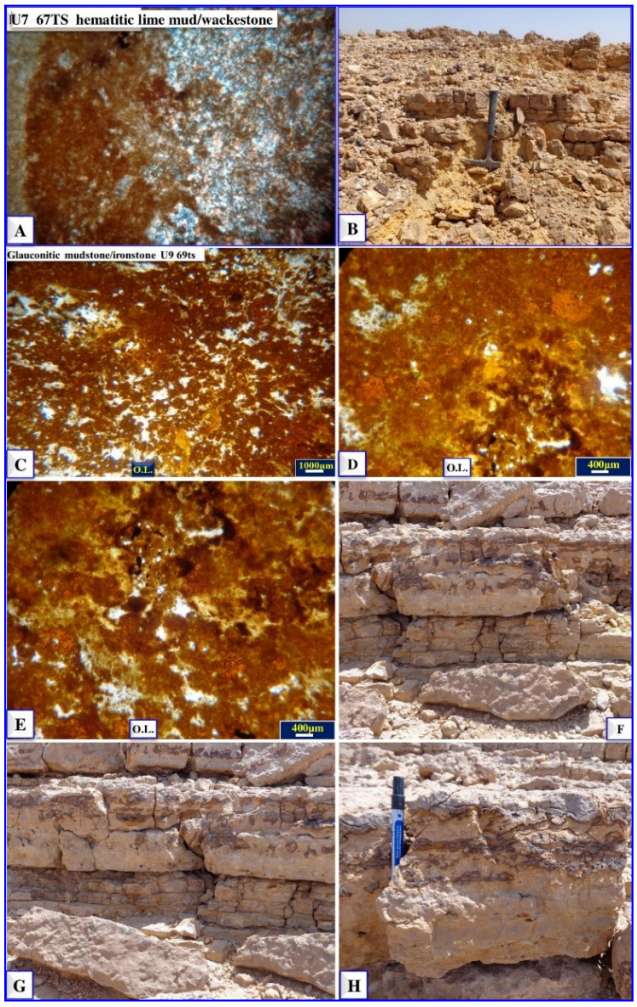

Fig. 5. (a and b): Hematitic lime mud/wackestone of the yellowish-green glauconitic mudstone-carbonate facies (F3) of the lower part of section I; (c and d): glauconitic mudstone/ironstone of the yellowish-green glauconitic mudstone-carbonate facies (F3); (e): progressive hematitization of iron-oxyhydroxides and formation of hematite (black); (f): chertified carbonates, microcrystalline quartz within organic-rich micrite; (g and h): geometry and cyclic nature of the yellowish-brown chert bands and laminae. O.L:. Ordinary Light, C.N.: Crossed Nicols.

2) Chertified Dolostone Facies (F4)

This chertified dolostone facies (F4) overlies the glauconitic mudstone-carbonate facies (F3), exhibited in Figures 3 and 5(f). It is composed of successive cycles; each cycle begins with light yellow fine dolostone or dolomitic mud grading upward into hard dolostone beds containing thin laminae and straight stringers of yellowish-brown chert (Figure 5(g)). Grading upward, the chert laminae and stringers become coalesced together, forming thicker bands and laminae (Figure 5(h)). In the uppermost parts of the cycles, thick continuous and /or discontinuous yellowish-brown chert bands and laminae are observed. Microscopically, it is composed of microcrystalline quartz that contains some calcitized dolomite relicts (Figure 6(a)). Some organic-rich micritic domains are still observed. The precursor organic-rich micritic domains showed progressive and subsequent stages of silicification and formation of microcrystalline quartz (Figure 6(b)).

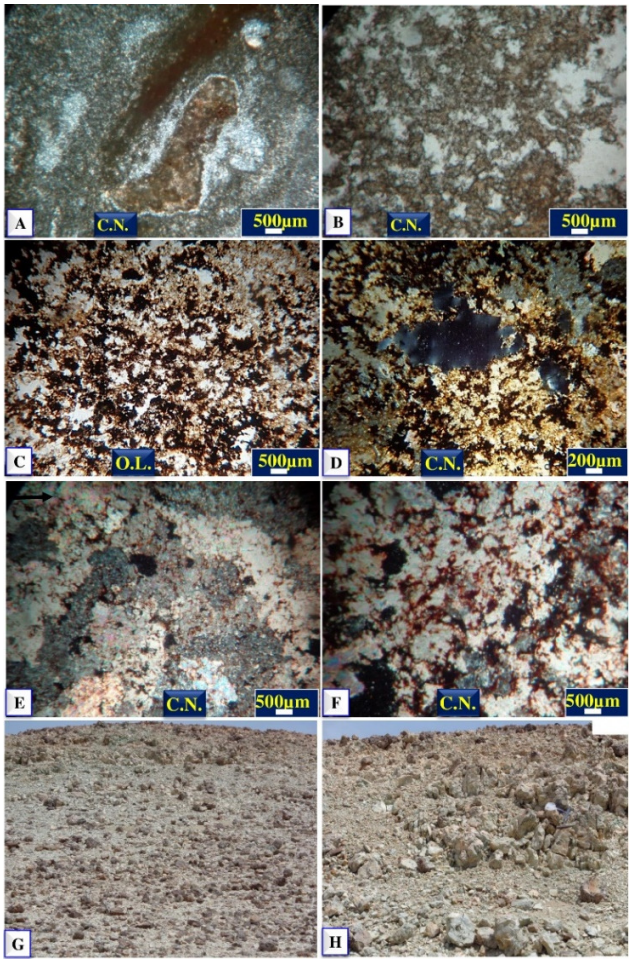

Fig. 6. (a): Chertified micrit/lime mud of the lower part of section I, (b): microcrystalline calcite formed by the recrystallization of organic-rich lime mud; (c): yellowish-brown chamositic iron clays with brown goethite and hematite with rare silt-sized quartz grains; (d): microcrystalline quartz replacing the iron oxide minerals; (e): blocky calcite probably formed by the calcification of Fe-dolomite; (f): hematite stringers (black) formed during the calcitization of the precursor Fe-dolomite rhombs and formation of block calcite; (h and h): green celadonitic tuffaceous mudstone facies (F6) of the green clays-iron ore (Unit 3). O.L:. Ordinary Light, C.N.: Crossed Nicols.

In normal hemipelagic chalk-chert successions, the formation of chert is interpreted to have been associated with marine high productivity conditions leading to the blooming of diatoms and radiolarians [6]. The close association of chert and carbonate and the replacement features suggest shallow marine conditions of deposition, and the occurrence of widely distributed relics of evaporites within the chert indicates that the conditions on this wide shelf probably fluctuated between normal marine and evaporitic conditions [6]. In the Gabal Um Himar succession, the condition of deposition is mainly restricted to lagoons, while the deposition of this succession is contemporaneous with volcanic activities. Therefore, the chert bands are similar in geologic situation in Wadi Girshah, Ablah area, Assir Terrain, Saudi Arabia. Similar situations of chert-carbonate succession were studied in [7-10].

3) Red Ferruginous Carbonate Facies (F5)

These facies terminate the first large cycle of the studied succession (Figure 3). They are composed of three characteristic small-scale cycles:

- The first cycle begins with yellow fine crystalline dolomitic mudstone (U12), which is overlain directly by a relatively thicker dolostone bed (U13).
- The second cycle is composed of yellowish green clays, which are overlain by a characteristic red bed (U14) and terminated by a bench-like dolostone bed (U16). The microscopic description of the red bed (U14) of the second cycle revealed its composition from yellowish brown chamositic iron clays, brown goethite, and hematite with rare silt-sized quartz grains, as shown in Figure 6(c). The goethite and hematite were formed by the diagenetic hematitization of the chamositic clays. Microcrystalline quartz is also observed to replace the iron oxide minerals (Figure 6d).
- The third cycle (U16, Figure 3) is composed of calcitized dolomite that contains some patches of blocky calcite formed by the calcitization of Fe-dolomite, as depicted in Figure 6(e). This is evidenced by the presence of hematite stringers formed during the calcitization of the precursor Fe-dolomite rhombs and the formation of blocky calcite (Figure 6(f)).

From the depositional environment point of view, the succession of the second cycle (Figure 3) shows deposition in slightly shallow lagoonal conditions, which is supported by the deposition of the green chamositic clays and the diagenetic oxidation of these clays into goethite and hematite. The green clays were previously postulated to be formed by the diagenetic degradation or transformation (neoformation) of primary allogenic clays of a kaolinite-goethite mixture with the addition of Mg2+ [18]. The formation of celadonite and glauconite minerals requires slightly oxygen-depleted conditions in a semi-confined micro-environment, facilitating the uptake of Fe into the structure. Furthermore, the composition of celadonite and glauconite is highly variable and is controlled by the availability of cations within the pore water micro-environment, while the major element composition of celadonite overlaps with that of evolved to highly evolved glauconite to a large extent.

C. Green Clays-Ironstones (Unit 3)

This unit is represented by the third (cycle 3) large-cycle (Figure 3). It comprises the following facies from base to top:

1) Green Celadonitic Tuffaceous Mudstone Facies (F6)

These facies attain up to 15 m (Figure 6(g)) and are composed mainly of thinly bedded green celadonitic clays, which are terminated by slightly oxidized green celadonitic clays/ or iron ore (Figure 6h). The lowermost part of this cycle (U17, Figure 7(a)) is composed mainly of amorphous green celadonitic clays, which show progressive stages of devitrification and the formation of microcrystalline quartz with very small relicts of green celadonitic clays, as portrayed in Figure 7(b). Hematitization of the green celadonitic clay led to the formation of blood-red goethite and hematite patches and domains. This is accompanied by the formation of microcrystalline quartz. Authors in [11] identified various species of Mg-clay minerals (stevensite, mixed-layer kerolite–stevensite, and sepiolite), along with calcite and dolomite.

2) Slightly Oxidized Green Clays (F7a)

Going toward the middle part of the third large cycle (cycle 3), the green clays become slightly oxidized (U18, Figure 7(c)). Microscopically, this horizon is composed mainly of yellowish-green oxidized celadonitic clays with some devitrified domains (microcrystalline quartz), as illustrated in Figures 7(d) and (e). Lamina is observed between the hematitized domains and the devitrified ones. The hematitized domains become highly oxidized, giving rise to goethite and hematite (Figure 7(f)). The devitrified patches are composed of crystalline quartz.

3) Highly Oxidized Green Clays -Ironstone (F7b)

This horizon is highly oxidized, and it is of a yellowish greenish brown color (U25, Figure 7(g)). It is present in the upper part of cycle 3 and is composed of highly devitrified celadonitic clays that contain reddish brown to black hematitic patches and domains (Figure 7(h)). The hematitic patches are composed mainly of blood-red amorphous goethite with black hematitic patches, as presented in Figure 8(a). Microcrystalline quartz patches are also observed. The light devitrified patches are either massive black domains or light devitrified ones that are composed of microcrystalline quartz (Figure 8(b)).

4) Highly Devitrified Celadonitic Clays (F8)

In these facies, the green clays become reddish green in color and highly devitrified (U27), as shown in Figures 8(b) and (c). The succession is composed of reddish brown, slightly oxidized, bench-like, reddish brown to black oxidized celadonitic clays (Figure 8(c)). The microscopic description of this part revealed its composition from peloid-like rounded patches and domains of slightly devitrified and hematitized tuffaceous mudstones (Figure 8(d)). The peloidal particles are either amorphous and hematitized or devitrified, as depicted in Figures 8(e) and (f). Some peloid-like patches are hematitized and devitrified. Close-up investigations of some of these bodies revealed their laminated nature, where domains of undevitrified ones are parallel to lighter devitrified ones (Figure 8(g)). Some peloids are hematitized from their peripheral parts, giving rise to superficial ooid-like bodies (Figure 8(h)). The central parts of these bodies are composed of amorphous silica (chalcedony). The outer reddish hematite zone becomes progressively corroded and replaced by amorphous silica, as shown in Figure 9(a). Intensive devitrification led to the progressive corrosion and embayment of the black peloids by the newly formed light microcrystals of quartz (Figure 9(b)). The devitrification of the different types of tuffs and the formation of new diagentic mineral phases, such as clinoptilolite + opal-C and clinoptilolite + mordenite + erionite + opal-C, was studied in [12-16].

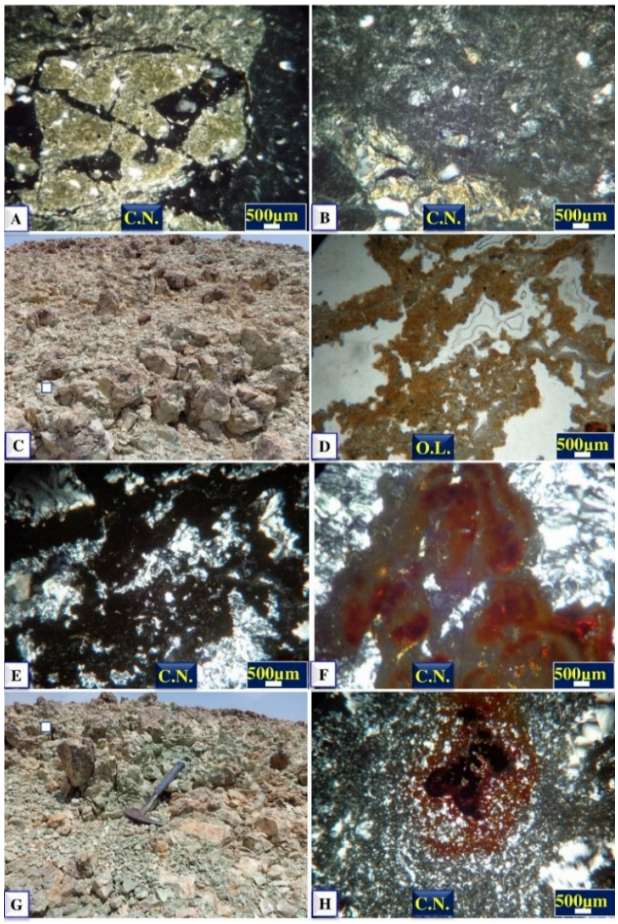

Fig. 7. (a): Amorphous green celadonitic clays; (b): devitrified formation of microcrystalline quartz with very small relicts of green celadonitic clays; (c) slightly oxidized green clays of facies F7; (d and e): yellowish green oxidized celadonitic clays with some devitrified domains (microcrystalline quartz (white); (f): highly oxidized green clays facies; (g): highly oxidized green clays facies (F7); (h): highly devitrified celadonitic clays containing reddish brown to black hematitic patches and domains (black). O.L:. Ordinary Light, C.N.: Crossed Nicols.

5) Ironstone Facies (F9)

a) Yellowish Green Subfacies (F9a)

The uppermost part of cycle 3 (Figure 3) is composed of rubble-like hematitic iron ore (Figures 3 and 9(c)). The systematic sampling and microscopic description of these Fe-ore facies revealed their formation during progressive and subsequent stages of diagenetic hematitization of precursor green celadonitic clays.

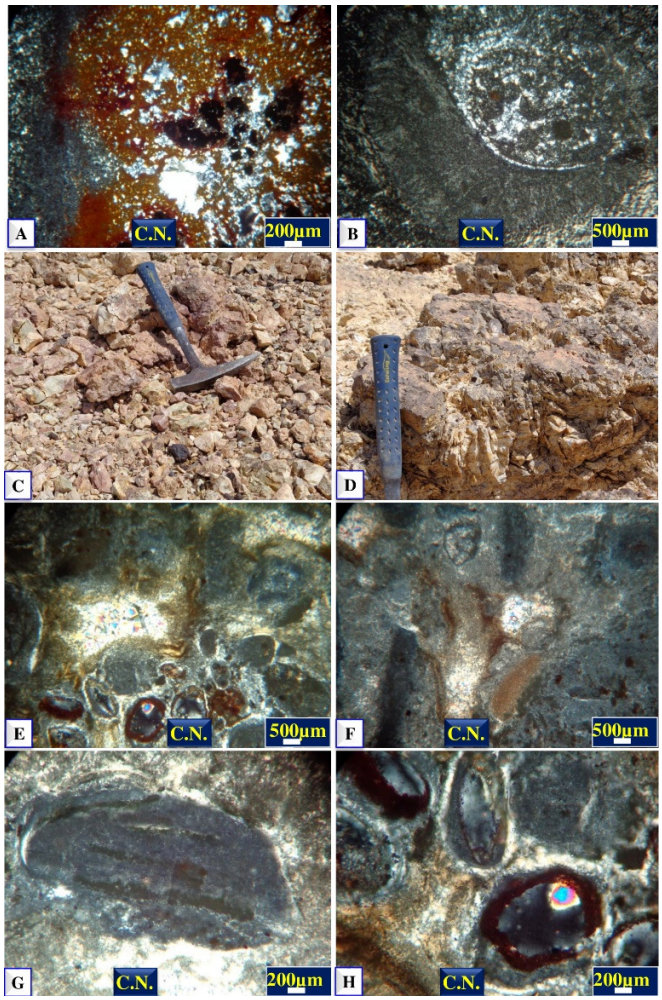

Fig. 8. (a): Hematitic patches composed mainly from blood-red amorphous goethite containing black hematitic patches; (b) lightly devitrified one composed of microcrystalline quartz; (c) reddish green color and highly devitrified celadonitic clays of F8; (d): reddish-brown slightly oxidized bench-like reddish brown to black oxidized celadonitic clays; (e): rounded patches and domains of slightly devitrified and hematitized peloids of tuffaceous mudstones; (f): peloidal particles, either amorphous and hematitized or devitrified; (g): peloid-like patches, hematitized and of laminated nature where domains of undevitrified patches are parallel to lighter devitrified ones; (h): hematitized peloids from their peripheral parts giving rise to superficial ooid-like bodies. O.L:. Ordinary Light, C.N.: Crossed Nicols.

b) Reddish Yellow Subfacies (F9b)

The progressive stage of hematitization of the precursor green celadonitic clays led to the formation of blood-red amorphous iron-oxyhydroxides (Figure 9(g)). During more progressive stages, the blood-red iron-oxyhydroxides get converted into a more red to reddish brown state (Figure 9(h)). This reddish-brown phase gets altered into dark brown to black hematite with relics of the blood-red amorphous iron oxyhydroxides. In some instances, the progressive hematitization was carried out as mottled stages where blood-red iron oxyhydroxides patches are still seen within the black hematite patches and domains, as shown in Figure 10(a).

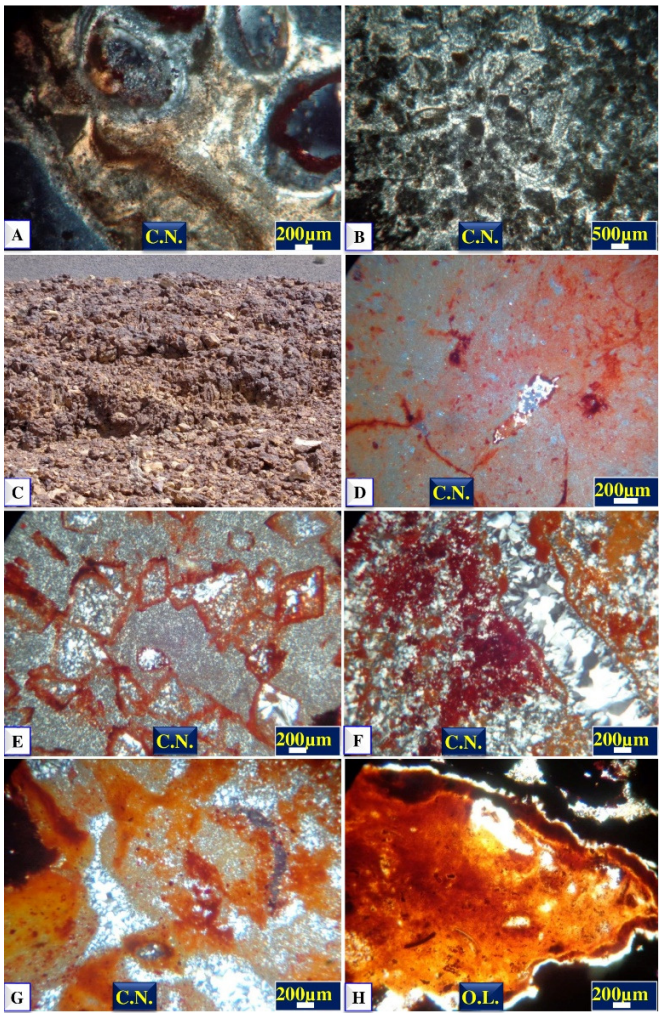

Fig. 9. (a) Central parts of these bodies are composed from amorphous silica (chalcedony), with the outer reddish hematite zone getting progressively corroded and replaced by the amorphous silica; (b) intensive devitrification led to the progressive corrosion and embayment of the black peloids by the newly formed microcrystals of quartz; (c): rubble-like hematitic iron ore in the topmost part of the measured section (F9); (d) initial stages of hematitization of the devitrified tuffs and the formation of hematite stain amorphous tuffs; (e) some rhomb-like devitrified domains are also observed unstained by the blood-red iron-oxyhydroxides; (f): hematitization associated with the irregular devitrification and formation of small quartz veins and veinlets; (g): progressive stage of hematitization of the precursor green celadonitic clays and the formation of blood-red amorphous iron oxyhydroxides; (h) blood-red iron oxyhydroxides converted into more red to reddish brown state. O.L:. Ordinary Light, C.N.: Crossed Nicols.

The initial stages of hematitization of the devitrified tuffs and the formation of amorphous tuffs stained by hematite are presented in Figure 9(d). At this stage, some white microcrystalline quartz stringers are observed unstained by the amorphous iron-oxyhydroxides. In addition, some rhomb-like devitrified domains are also observed (Figure 9(e)). The devitrified patches are present as rhombohedra that are surrounded by rim hematitic zones. The formation of these rhombs is mainly related to the diagenetic processes. The blood iron oxy-hydroxides surrounding the microcrystalline rhombs become progressively hematitized, giving rise to a black

hematite zone. In some cases, this hematitization is almost associated with the irregular devitrification and the formation of small quartz veins and veinlets (Figure 9(f)).

c) Highly Silicified-Chertified (Devitrified) Subfacies (F9c)

The iron ore of facies F9b is changed laterally into a light, highly silicified horizon and is composed mainly of devitrified tuffs which contain ooid-like bodies of microcrystalline quartz (Figure 10(b)). These ooids are embedded in less devitrified dark tuffs (Figure 10(c)). In some cases, the ooids become entirely devitrified and are composed mainly of interlocked quartz grains. Intensive recrystallization led to the formation of coarse-crystalline domains (Figure 10(d)).

d) Reddish Brown Ironstone Subfacies (F9d)

The topmost part of cycle 3 (U29) is mainly composed of reddish brown to black iron ore horizon containing some lighter, highly silicified patches and domains (Figure 10(e)). The field observations revealed that this iron ore horizon is composed of successive cycles, each cycle begins with lighter parts and is terminated with ledge-forming reddish brown to black iron ore benches (Figure 10(f)). The basal part contains some white-colored silicified domains. The microscopic description of the lower parts of these cycles revealed their composition from highly devitrified tuffs that contain less frequent slightly oxidized yellowish green celadonitic clays (Figure 10(g)). The oxidized parts are recrystallized and hematitized, giving rise to reddish brown to black hematite patches and domains (Figure 10(h)). The middle parts of the cycles are composed mainly of green celadonitic clays that show incipient stages of diagenetic hematitization and calcitization, giving rise to blood-red iron oxyhydroxides interlocked with blocky calcite (Figure 11(a)). Towards the middle parts, the green celadonitic clays become in situ pelletized and hematitized, giving rise to blood-red iron oxyhydroxides (Figure 11(b)). Highly corroded and embayed white quartz grains are observed embedded within the blood-red iron oxyhydroxides.

The progress of hematitization led to the homogenization of the hematitized peloids, which led to the formation of large amorphous iron oxyhydroxide domains. The progressive dehydration and recrystallization of the blood-red amorphous iron-oxyhydroxide phase led to the formation of large in situ-formed ooids of gradational contact with the enclosing matrix (Figure 11(c)). The continuation of the aforementioned process led to the formation of well- developed ooids of reddish-brown goethite (Figure 11(d)). The quartz grains become tangentially arranged in ooid-like forms. The diagenetic hematitization led to the formation of mottled dark brown to black hematite patches and blood-red lighter goethitic patches (Figure 11). In this horizon, incompletely hematitized semi-rounded patches (peloid-like) are still preserved within the highly hematitized zone. In these patches, the slightly hematitized peloids become intensively corroded and embayed by the calcite cement. Lighter yellowish-green domains are still preserved within the highly hematitized zones (Figure 11). Some lighter and slightly hematitized domains are present in the highly hematitized patches. These lighter zones become progressively hematitized. This is accompanied by the more hematitization (darkening) of the previously hematitized zones (Figure 12). In more advanced stages of hematitization, the lighter domains become completely hematitized. Very small relics of unhematitized patches are still observed (Figure 12).

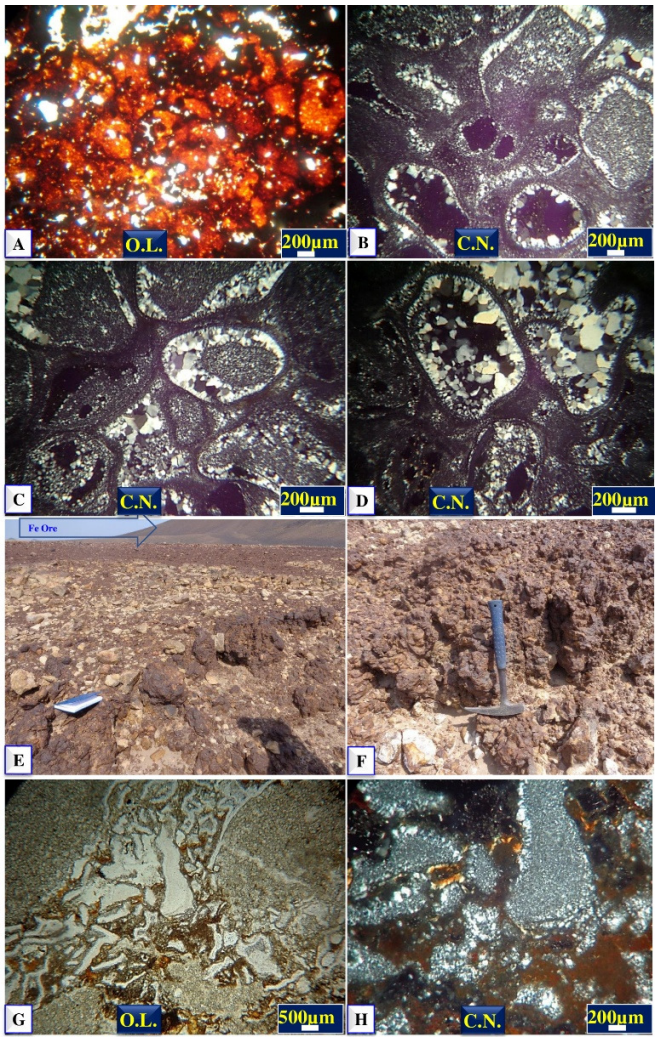

Fig. 10. (a): Formation of blood-red iron oxyhydroxides patches within the black hematite patches and domains; (b): devitrified tuffs with ooids-like bodies of microcrystalline quartz; (c): quartz ooids embedded in less devitrified dark tuffs; (d) ooids entirely devitrified and composed mainly from interlocked quartz grains; (e): reddish-brown to black iron ore horizon containing some lighter highly silicified patches and domains; (f): cycles of the iron ore subfacies, terminated with ledge-forming reddish brown to black iron ore benches; (g): highly devitrified tuffs containing less frequent slightly oxidized yellowish-green celadonitic clays; (h): recrystallized and hematitized tuffs giving rise to reddish brown to black hematite patches and domains. O.L:. Ordinary Light, C.N.: Crossed Nicols.

During these stages of hematitization, in situ formed pseudo-ooids were formed within the amorphous iron-oxyhydroxides, as exhibited in Figure 12. There is no sharp contact between these ooids and the enclosing matrix, which supports their formation during subsequent stages of diagenetic recrystallization of the associated blood-red amorphous iron-oxyhydroxides. Ultimate stages of hematitization led to the

complete hematitization of the ooid and the enclosing matrix, leaving small patches of microcrystalline calcite (Figure 12(d)). Facies F6, F7, F8, and F9 represent a green celadonitic clay succession that is composed mainly of green mudstones that show different stages of hematitization and devitrification from the lower to the middle and upper part of cycle 3 (Figure 3).

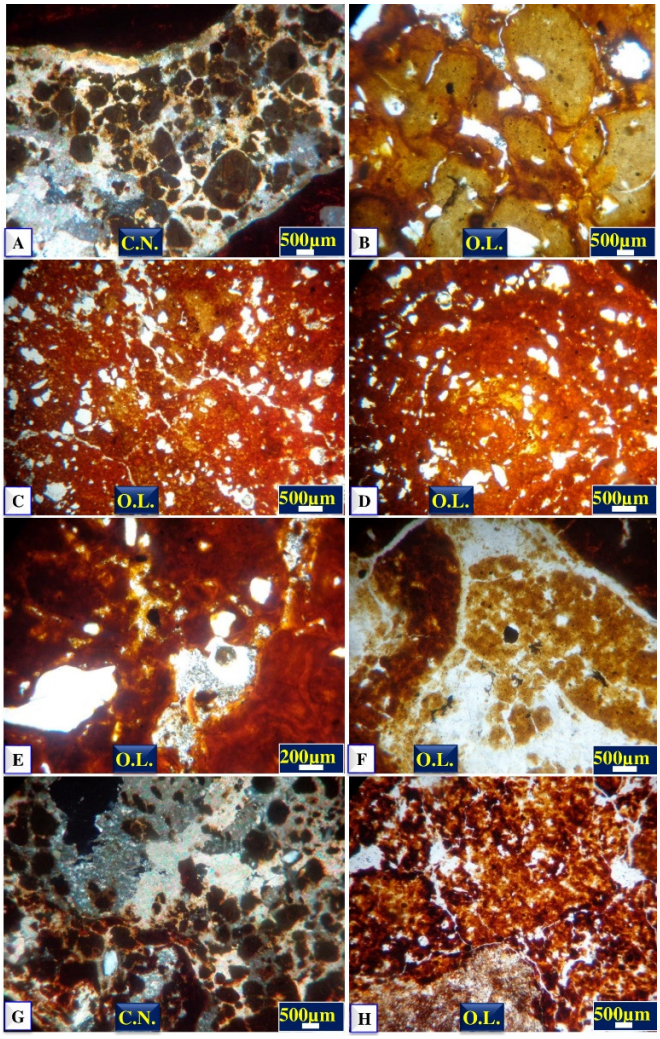

Fig. 11. (a): Diagenetic hematitization and calcitization giving rise to blood-red iron-oxyhydroxides interlocked with blocky calcite; (b): in situ pelletization and hematitization of the green celadonitic clays; (c): in situ formed ooids of gradational contact with the enclosing matrix; (d) formation of well-developed ooids of reddish brown goethite; (e): formation of mottled dark brown to black hematite patches and blood-red lighter goethitic patches; (f): semi-rounded patches (peloid-like) still preserved within the highly hematitized zone; (g): slightly hematitized peloids, intensively corroded and embayed by the calcites cement; (hs) lighter slightly hematitized domains. O.L:. Ordinary Light, C.N.: Crossed Nicols.

In slightly deeper areas, during the new marine transgression after the deposition of the succession of cycle 2 (Figure 3), the deposited tuffaceous materials were converted into green celadonitic clays during synsedimentary and diagenetic processes. These green clays were formed as a result of the degradation of the basic tuffs into their original elements, where Si, Al, Fe, and Mg were released and reacted together, forming green authigenic clays of different compositions according to the level and concentration of these elements in the depositional environments [5]. These clays were subjected to diagenetic hematitization below the sediments-water interface, leading to the formation of yellowish green, yellow, and reddish brown oxidized clays according to the composition of the original precursor clays before the hematitization [5]. The initially formed iron-bearing minerals are amorphous iron-oxyhydroxides. The progressive stages of diagenetic dehydration and recrystallization of these amorphous Fe-oxyhydroxides and /or the green glauconitic clays led to the formation of goethite and hematite in different fabrics.

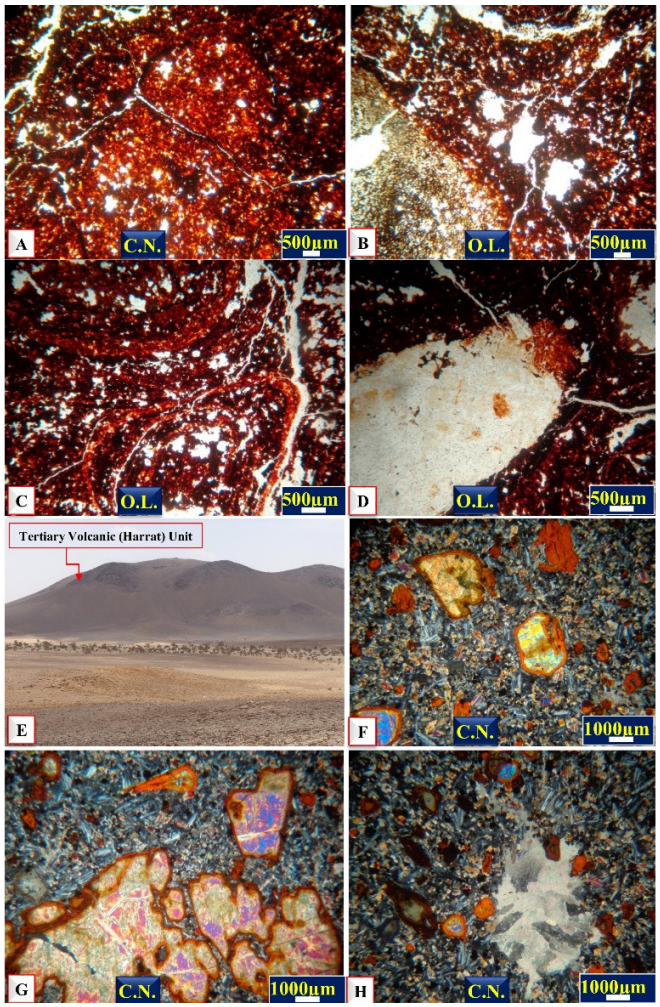

Fig. 12. (a) Progressive hematitization accompanied by the more hematitization (darkening) of the previously hematitized zones; (b) very small relicts of unhematitized patches are still observed; (c): in situ formed pseudo-ooids formed within the amorphous iron oxyhydroxides; (d): ultimate stages of hematitization of the ooids and the enclosing matrix leaving small patches of microcrystalline calcite; (e): tertiary basaltic flows of Unit 4; (f) large percent of Ca-plagioclase, olivines and pyroxenes in basalt; (g): intensive hematization of olivines and pyroxenes giving rise to blood-red amorphous iron oxyhydroxides; (h) large patched of blocky calcite formed instead of the Ca-plagioclase crystals and the interstitial glassy materials. O.L:. Ordinary Light, C.N.: Crossed Nicols.

D. Tertiary Volcanic (Harrat) (Unit 4)

This unit attains up to 60 m thickness and is composed in its lower parts of successive interbedded tuffaceous mudstones and siltstones and basalt (Figures 3 and 12(e)). Towards the upper parts, it is composed of basalts of variable crystal sizes and colors. The microscopic description of these basalts revealed their composition from a large percentage of Ca-plagioclase, olivines, and pyroxenes (Figure 12(f)). Most of the observed olivines and pyroxene crystals are intensively hematitized, giving rise to blood-red amorphous iron oxyhydroxides (Figure 12(g)). Large patches of blocky calcite were formed instead of the Ca-plagioclase crystals, as well as the interstitial glassy materials (Figure 12(h)). These tertiary basic volcanics are still under further stratigraphic and petrographic consideration.

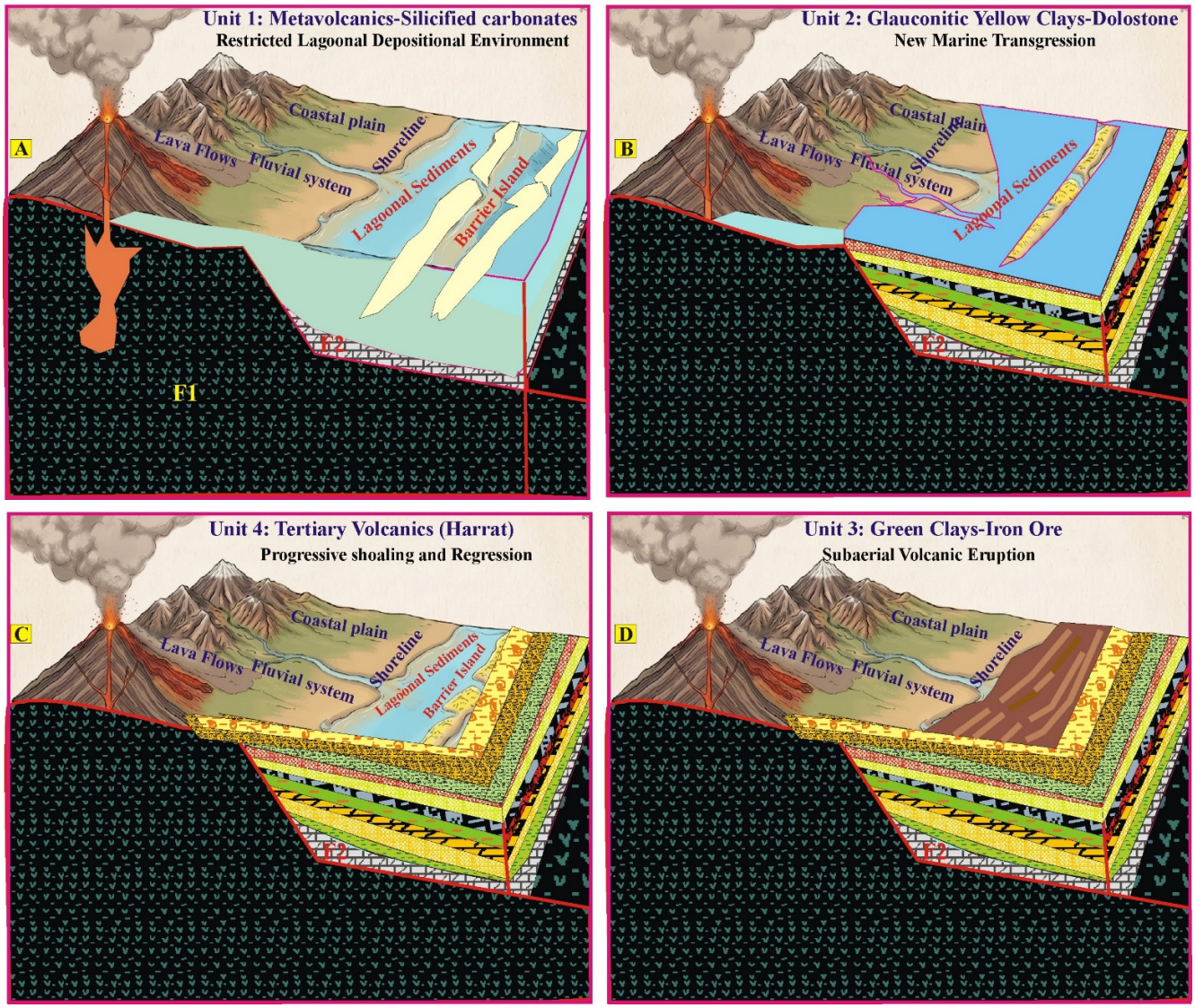

Fig. 13. Depositional model: (a) deposition of Unit 1, (b) deposition of Unit 2, (c) deposition of Unit 3, and (d) deposition of Unit 4.

IV. FACIES ASSOCIATIONS AND DEPOSITIONAL MODEL

The studied sedimentary succession of the Um Himar Formation in the measured section is very thin and of characteristic lithology. It is subdivided into four main units and nine facies and related subfacies. Similar mixed carbonate-volcaniclastic facies represent shallow marine environments from the middle ramp to shallow subtidal environments in the inner ramp in the Carboniferous units in southern Mexico [17]. The depositional model of the studied succession is demonstrated in Figure 13. Unit 1 represents part of the Arabian shield rocks and deposition of silicified carbonates during periods of very low input of volcaniclastics in restricted lagoonal environments (Figure 13(a)). Unit 2 contains egg-yellow oxidized glauconitic clays and siltstones, which indicates deposition in dysaerobic conditions followed by diagenetic hematitization of the glauconitic clays [5]. These

clays are followed upward by egg-yellow bedded dolostones formed by the syn-depositional-early diagenesis of Ca, Mg, Fe-rich lime mud. These dolostone beds are highly chertified and contain continuous and discontinuous laminae and beds of chert.

The formation of chert indicates restricted and saline water. This is also indicated by the presence of calcitized red ferroan dolomite of facies F5. This unit was deposited during a new marine transgression with general upward shoaling and the formation of restricted environments during which chertified carbonates were deposited (Figure 13(b)). Unit 3 was deposited during new marine regressive events, where green celadonitic clays were formed (cycle 3, Figure 13(c)). These clays can be correlated laterally by contemporaneous volcanic eruption. The celadonitic clays are similar to the green glauconitic clays in their deposition in a dysaerobic depositional environment, but they differ only in their Mg and Fe content as well as their formation instead of precursor tuffaceous volcanic materials and not instead of degraded clays as the glauconitic clays [5].

Toward the upper part of the green clay unit, these clays become bedded and slightly to highly oxidized facies of F7 and F8. This indicates deposition during progressive shoaling and decreasing of the water column, mostly confirmed by the complete oxidation and devitrification of these celadonitic clays and the formation of the iron ore of facies F9 in the uppermost part of this unit. Unit 4 was formed where the study area was uplifted, and a thick succession of Tertiary volcanics and the intercalated volcaniclastics occurred (Figure 13(d)). The contact between these volcanics and the underlying succession is still under investigation to confirm whether it is a normal gradational or erosional contact of the hiatus period.

V. DISCUSSION AND CONCLUSIONS

According to the stratigraphic, facies analyses, and depositional environments, the study reached the following conclusions:

- The studied succession was described in [3]. It was related to deposition during the Paleocene time in estuarine or lagoonal environments, while the climate was either tropical or subtropical, probably seasonally arid in the nearby interior. This scenario was developed on the basis of the presence of certain vertebrates, their fossilized condition, and the type of sediments in which they were deposited. Oolitic ironstone beds within the succession were also described [8].
- The studied succession of the Um Himar Formation represents an ideal example of volcanism and the syn-contemporaneous sedimentation. The deposited volcanic derivatives suffered syn-depositional degradation and formation of new mineral phases according to the loci of the depositional site and the predominant micro physico-chemical conditions.
- The small thickness of the studied succession, as well as the absence of any unconformity surface or erosional surface contact between the so-called Tertiary succession and the underlying Precambrian metavolcanics argue against the Tertiary age of this succession.
- The studied succession was assigned to be of Paleocene-Oligocene age based on the Odontaspis, Ginglymostoma, Myliobatids, Catfish, dinosaurs, and lungfish Ceratodus identified in [3], suggesting nearshore or estuarine shallow waters for the deposition of the succession.

The present study recognizes only some small vertical and inclined burrows and some freshwater gastropods, which are described in chert and carbonate beds in other areas, and these will be the subject of more intensive further study. The presence of green celadonitic clays and the tuffaceous mudstone units, as well as the recorded glass shards with the different petrographic lithotypes, indicated the presence of basic volcanic activities nearby within the depositional basin. This is supported by the presence of tuffaceous ironstones and tuffaceous mudstone intercalation within the studied ironstones of the Um Himar Formation [8].

The studied succession is correlated with another section measured 4 km to the east of this section, and it is observed that the two sections are not similar from the stratigraphic and sedimentological points of view. In the second section, oolitic ironstone beds, bedded dolomitic carbonates, and basaltic flows are recorded. The classification and origin of these oolitic ironstone beds were studied in [8]. Similar Miocene mixed carbonate–pyroclastic sedimentation was described in the Central Basin, Iran [18]. It was concluded that carbonates were deposited in shallow-water high-energy conditions mostly as reef and fore-reef facies, while the Carbonate deposition took place on a carbonate ramp under conditions of periodic to almost continuous influx of pyroclastic material. Also, lower cretaceous mixed siliciclastic-carbonate-tuffaceous and organic-rich deposits were described in [13] in the Jiufotang formation in the Luxi sag, Songliao basin.

The Um Himar area represents the first described tertiary succession, and is described in the present study to confirm the interplay between the Tertiary volcanic flows. In addition, authors in [8] confirmed the strong relation between volcanic ash and different types of oolitic ironstones.

DECLARATION OF COMPETING INTERESTS

The authors declare no competing interests.

ACKNOWLEDGMENT

The project was funded by the Deanship of Scientific Research (DSR), King Abdulaziz University, Jeddah, under Grant No. 374/145/1433. The authors sincerely acknowledge the technical and financial support provided by DSR.

DATA AVAILABILITY

Not applicable to this work.

REFERENCES

[1] G. T. Madden, I. M. Naqvi, F. C. Whitmore, D. L. Schmidt, W. Langston, and R. C. Wood, "Paleocene Vertebrates from Coastal Deposits in the Harrat Haden Area, at Taif Region, Kingdom of Saudi Arabia," U. S. Geological Survey, Virginia, USA, Technical Report Open-File Report 80-227, 1979.

[2] P. R. Johnson, "Explanatory Notes to the Map of Proterozoic Geology of Western Saudi Arabia," Saudi Geological Survey, Jeddah, Kingdom of Saudi Arabia, Technical Report SGS-TR-2006-4, 2006.

[3] A. A. Mesaed, M. Gameil, and R. F. Thiga, "Stratigraphic Setting, Facies Types, and Mineral Paragenesis of the Carbonate-Bearing Tertiary Sedimentary Succession of Usfan Area, West-Central Saudi Arabia," *Engineering, Technology & Applied Science Research*, vol. 15, no. 6, pp. 28818–28828, Dec. 2025, https://doi.org/10.48084/etasr.13394.

[4] G. T. Madden, "Paleocene Pycnodont Fishes from Jabal Umm Himar, Harrat Hadan Area, Kingdom of Saudi Arabia," U. S. Geological Survey, Virginia, USA, Technical Report Open-File Report 83-453, 1983.

[5] C. Frank, Jr. Whitmore, and C. T. Madden, "Paleocene vertebrates from Jabal Umm Himar, Kingdom of Saudi Arabia," U.S. Geological Survey, Virginia, USA, Technical Report Bulletin 2093, 1995.

[6] S. Moshkovitz, A. Ehrlich, and D. Soudry, "Siliceous Microfossils of the Upper Cretaceous Mishash Formation, Central Negev, Israel," *Cretaceous Research*, vol. 4, no. 2, pp. 173–194, Jun. 1983, https://doi.org/10.1016/0195-6671(83)90048-4.

[7] H. Lei, W. Huang, Q. Jiang, and P. Luo, "Siliceous Deposition in Limestone-Marl Alternations of the Yangtze Carbonate Platform During the Permian Chert Event," *Palaeogeography, Palaeoclimatology, Palaeoecology*, vol. 651, Oct. 2024, Art. no. 112382, https://doi.org/10.1016/j.palaeo.2024.112382.

[8] R. J. Taj, A. A. Mesaed, M. I. Matsah, and M. Gameil, "Origin and Mechanism of Formation of the Oligo-Miocene Ironstones of Umm Himar Formation, Turabah Area, Southwestern Arabian Shield, Saudi Arabia," *Arabian Journal of Geosciences*, vol. 10, no. 15, Aug. 2017, Art. no. 322, https://doi.org/10.1007/s12517-017-3091-0.

[9] R. Okhravi and A. Amini, "An Example of Mixed Carbonate–Pyroclastic Sedimentation (Miocene, Central Basin, Iran)," *Sedimentary Geology*, vol. 118, no. 1–4, pp. 37–54, Jun. 1998, https://doi.org/10.1016/S0037-0738(98)00004-9.

[10] Y. Li, J. Xue, S. Wang, Z. Ye, and J. Yang, "Mixed Siliciclastic-Carbonate-Tuffaceous Sedimentation in a Rift Lacustrine Basin: A Case Study of the Lower Cretaceous Jiufotang Formation in the Luxi Sag, Songliao Basin," *Marine and Petroleum Geology*, vol. 164, Jun. 2024, Art. no. 106851, https://doi.org/10.1016/j.marpetgeo.2024.106851.

[11] P. Singh, S. Banerjee, T. R. Choudhury, S. Bhattacharya, and K. Pande, "Distinguishing Celadonite from Glauconite for Environmental Interpretations: A Review," *Journal of Palaeogeography*, vol. 12, no. 2, pp. 179–194, Apr. 2023, https://doi.org/10.1016/j.jop.2023.02.001.

[12] L. De Pablo-Galán and M. D. L. Chávez-García, "Diagenesis of Oligocene Vitric Tuffs to Zeolites, Mexican Volcanic Belt," *Clays and Clay Minerals*, vol. 44, no. 3, pp. 324–338, Jun. 1996, https://doi.org/10.1346/CCMN.1996.0440303.

[13] D. Cicerali *et al.*, "Mineralogy, Chemistry, and Genesis of Zeolitization in Eocene Tuffs from the Bayburt Area (NE Turkey): Constraints on Alteration Processes of Acidic Pyroclastic Deposits," *Journal of African Earth Sciences*, vol. 162, Feb. 2020, Art. no. 103690, https://doi.org/10.1016/j.jafrearsci.2019.103690.

[14] B. Bai *et al.*, "Devitrification-Driven Pore Formation in the Tight Tuff from the Tiaohu Formation in the Santanghu Basin, Northwest China," *Scientific Reports*, vol. 16, no. 1, Jan. 2026, Art. no. 3491, https://doi.org/10.1038/s41598-025-30673-3.

[15] H. Hong *et al.*, "Volcanic Sources and Diagenetic Alteration of Permian–Triassic Boundary K-Bentonites in Guizhou Province, South China," *Palaeogeography, Palaeoclimatology, Palaeoecology*, vol. 519, pp. 141–153, Apr. 2019, https://doi.org/10.1016/j.palaeo.2018.01.019.

[16] N. Gong *et al.*, "Influences of Sedimentary Environments and Volcanic Sources on Diagenetic Alteration of Volcanic Tuffs in South China," *Scientific Reports*, vol. 8, no. 1, May 2018, Art. no. 7616, https://doi.org/10.1038/s41598-018-26044-w.

[17] S. Guerrero-Moreno, L. A. Solari, J. C. Castillo-Reynoso, and M. A. Torres-Martínez, "Paleoenvironmental Evolution of a Carboniferous Marine Succession During Active Volcanism in Southern Mexico and Its Implications in the Western Pangea Margin Configuration," *Journal of South American Earth Sciences*, vol. 129, Sep. 2023, Art. no. 104476, https://doi.org/10.1016/j.jsames.2023.104476.

[18] S. Goswami, "Genetic Link Between Banded Iron Formation (BIF), Tuff, and Chert in a Volcano-Sedimentary Environment of Archaean Greenstone Belts," *Discover Geoscience*, vol. 3, no. 1, Dec. 2025, Art. no. 236, https://doi.org/10.1007/s44288-025-00343-y.